

PDF computations for power-in-the-bucket measurements of an IR laser beam propagating in the maritime environment

C. Nelson^{*a,d}, S. Avramov-Zamurovic^a, R. Malek-Madani^a, O. Korotkova^b, R. Sova^c, F. Davidson^d

^aThe United States Naval Academy, 121 Blake Road, Annapolis, MD 21402, USA

^bThe University of Miami, Coral Gables, FL, 33124 USA

^cThe Johns Hopkins University Applied Physics Laboratory, 11100 Johns Hopkins Road, Laurel, MD 20723, USA

^dThe Johns Hopkins University, 3400 N. Charles Street, Baltimore, MD 21218, USA;

ABSTRACT

During two separate field tests (July and September 2009) the performance of a free-space optical (FSO) communications link was evaluated in the maritime environment off of the mid-Atlantic coast near Wallops Island, VA. During these two field tests, a bi-directional shore-to-ship data link was established using commercially available adaptive optics terminals. The link, which ranged from 2 – 22 km (optical horizon), was established between a lookout tower located on Cedar Island, VA and a Johns Hopkins University Applied Physics Laboratory research vessel. This paper presents statistical analysis of the power-in-the-bucket captured from two detectors placed alongside the adaptive optics terminal during the September 2009 field trial. The detectors ranged in size from 0.25” to 1.0” in diameter. We will present the histogram reconstruction and compare the data for the 0.25” and 1.0” power-in-bucket (PIB), and 1.0” power-in-fiber (PIF) Adaptive Optics (AO) detectors with analytical probability density function (PDF) models based on the Lognormal, Gamma-Laguerre, and Gamma-Gamma distributions. Additionally, dependence of the results on propagation distance, detector aperture size, and varying levels of optical turbulence are investigated.

Keywords: Free-space optical communications, maritime communications, Gamma-Laguerre, Gamma-Gamma, probability density function, atmospheric turbulence, scintillation

1. INTRODUCTION

As highlighted and discussed by Juarez, et al at this conference in 2010 and by Das, et al at Milcom in 2008 [1,2], the U.S. Navy relies heavily on radio frequency (RF) communication networks. This reliance generates two major operational limitations: bandwidth, and lack of contingency capability in the event of jamming or detection by adversaries. One possible complimentary solution to current RF systems is through the use of free-space optical (FSO) communication links. Free-space optical communication links are inherently high-bandwidth as well as highly directional, which makes them hard to detect or jam.

A laser beam propagating in a maritime environment faces significant challenges, notably from random and significant intensity fluctuations driven by optical turbulence along the propagation path [3]. In 2009, The Johns Hopkins University Applied Physics Laboratory (JHU/APL) developed and executed an internal research and development effort to assess hybrid RF/optical communication links in the maritime environment. This paper focuses on the probability density function (PDF) for infrared (IR) data collected during the September 2009 field test. Specifically, can we best determine the PDF in the maritime environment as a:

- 1) Function of propagation distance
- 2) Function of three optical detectors – 0.25”, 1.0”, as well as for a 1.0” Adaptive Optics (AO) Terminal
- 3) Function of varying levels of optical turbulence.

The PDF of the intensity for a given detector is critical for understanding the fade statistics of an optical signal through the bit-error rate (BER). Understanding the evolution and form of the PDF as it relates to distance, turbulence level, and detector size holds great benefit for optimizing the maritime communication link in a given optical channel.

*cnelson@usna.edu; phone 410-293-6164; fax 443-778-0619; www.usna.edu

2. EXPERIMENT DESCRIPTION

Figure 1 below illustrates the shore-to-ship, bi-directional optical link as described in the abstract. Figure 2 below illustrates the experimental set-up.



Figure 1 – Experimental set-up overview. (a) Test Run path overview [4]. (b) View from tower

During active operation, the beam center was locked onto the 1.0” Adaptive Optics (FSO) apertures of both terminals (Tower and Chessie). Additional details of the experimental configuration and channel characterization can be found in the SPIE paper by Juarez et al, presented at this conference in 2010 [1].

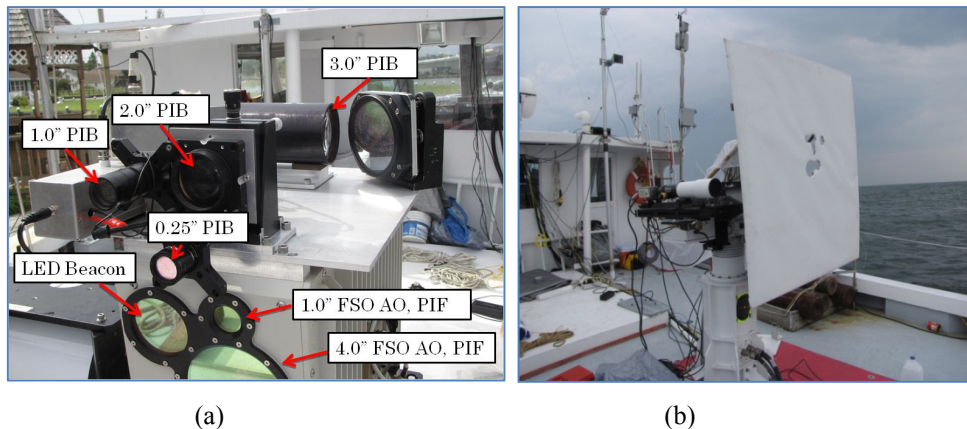


Figure 2 – a) 0.25” – 3.0” Power-in-Bucket (PIB) detectors as well as the 1.0” and 4.0” PIF AO (FSO) set-up on Chessie. b) 4 ft. x 4 ft. screen for IR imaging installed in front of PIB detectors.

3. THEORETICAL BACKGROUND

The Probability Density Function, W , of the fluctuating intensity, I , gives the probability that the beam’s intensity attains a certain level as described in the following equations where the intensity is normalized by its mean value.

$$Probability(a < I < b) = \int_a^b W(I) dI \quad (1)$$

The higher order statistical moments are obtained from the following:

$$\langle I^{(n)} \rangle = \int_0^\infty W(I) I^n dI \quad (2)$$

Several PDF models have been suggested for light propagation in random media. We are concerned with three models, the Lognormal (LN) [5], Gamma-Laguerre (GL) [6], and the Gamma-Gamma (GG) [7].

The approach introduced by Barakat in reference [6] and discussed in [8,9] as the Gamma-Laguerre (GL) PDF model is defined as follows. It utilizes the Gamma distribution weighted by generalized Laguerre polynomials and has the form:

$$W_{GL}(I) = W_g(I) \sum_{n=0}^{\infty} W_n L_n^{(\beta-1)}\left(\frac{\beta I}{\mu}\right), I \geq 0 \quad (3)$$

Where $W_g(I)$ is the Gamma distribution given by:

$$W_g(I) = \frac{1}{\Gamma(\beta)} \left(\frac{\beta}{\mu}\right)^{\beta} I^{\beta-1} \exp\left(-\frac{\beta I}{\mu}\right) \quad (4)$$

With Γ being the Gamma function and the two parameters of the distribution defined by the first and second moments.

$$\mu = \langle I \rangle, \quad \beta = \langle I \rangle^2 / (\langle I^2 \rangle - \langle I \rangle^2) \quad (5)$$

Additionally, W_n are the weighting coefficients given by:

$$W_n = n! \Gamma(\beta) \sum_{k=0}^n \frac{(-\beta/\mu)^k I^k}{k!(n-k)! \Gamma(\beta+k)}, \text{ and } W_0 = 1, W_1 = W_2 = 0. \quad (6)$$

The generalized Laguerre Polynomials, $L_n^{(\beta-1)}(x)$ as used in formula (3) are given by:

$$L_n^{(\beta-1)}(x) = \sum_{k=0}^n \binom{n+\beta-1}{n-1} \frac{(-x)^k}{k!} \quad (7)$$

In the original paper by Barakat [6], the author recommends using the first five moments of the data to help ensure accurate and stable approximations of the PDF. The Gamma-Laguerre model relies only on the first several statistical moments of the data and an assumption of being a unimodal PDF. The GL method does not require any knowledge of the atmospheric parameters or characteristics with regards to the source, propagation distance, or atmospheric spectrum.

An alternate model suggested in reference [7] has become known as the Gamma-Gamma (GG) PDF model. In contrast to the GL method, the GG PDF model requires knowledge of a number of atmospheric and source parameters such as propagation distance, atmospheric spectrum, and beam width at launch. The GG PDF model has the following form:

$$W_{GG}(I) = \frac{2(\alpha\beta)^{\frac{\alpha+\beta}{2}}}{\Gamma(\alpha)\Gamma(\beta)} I^{\frac{\alpha+\beta}{2}-1} K_{\alpha-\beta}(2\sqrt{\alpha\beta I}), I > 0 \quad (8)$$

Where $\Gamma(x)$ is the Gamma function as before, $K_m(x)$ is the modified Bessel function of the second kind, and where the parameters α and β are defined as follows:

$$\alpha = \frac{1}{\exp(\sigma_{lnx}^2)-1}, \quad \beta = \frac{1}{\exp(\sigma_{lny}^2)-1} \quad (9)$$

With σ_{lnx}^2 and σ_{lny}^2 are normalized variances of intensity due to perturbations caused by large and small scales of the turbulent medium. Under the assumption of the Kolmogorov power spectrum these quantities are given by [10]:

$$\sigma_{lnx}^2 = \frac{0.49\sigma_B^2}{[1+0.56(1+\vartheta)\sigma_B^5]^{7/6}} \quad \text{and} \quad \sigma_{lny}^2 = \frac{0.51\sigma_B^2}{[1+0.69\sigma_B^5]^{5/6}} \quad (10)$$

Here σ_B^2 is the normalized variance of fluctuating intensity or scintillation index and given by the following expression, $\sigma_B^2 = (\langle I^2 \rangle - \langle I \rangle^2) / \langle I \rangle^2$, and $\vartheta = [1 + (\frac{2L}{kW_0^2})^2]^{-1}$ is the refraction parameter, W_0 is the initial launch beam radius (5 cm), L is the propagation distance from the source to receiver, and $k = 2\pi/\lambda$ is the wave number.

One additional model used for comparison is the Lognormal distribution given as follows [5]:

$$W_{LN}(I) = \frac{1}{I\sigma\sqrt{2\pi}} \exp\left[-\frac{[\ln(I)-\mu]^2}{2\sigma^2}\right], I > 0 \quad (11)$$

Where μ is the mean and σ^2 is the variance of the log-irradiance: $\mu = \langle \ln(I) \rangle$ and $\sigma^2 = \text{var}(\ln(I))$.

4. RESULTS

Two cases are presented, low and low-moderate optical turbulence conditions over varying distance in the maritime environment. In each case the data histogram, Lognormal (LN), Gamma-Gamma (GG), and Gamma-Laguerre (GL) PDF fits are computed directly from moments of the data, and are presented for a 1.0" aperture Power-in-Fiber (PIF) Adaptive Optics (AO) terminal and 0.25", and 1.0" aperture Power-in-Bucket (PIB) detectors. The generated runs are each one minute in duration, the Chessie's average speed was just over 2 m/s, and the samples of data were collected at 10,000 samples/sec or 600,000 data points for the one minute. Additionally, the Least Square Error (LSE) fits for each distribution, as well as the LSE tail fits (1st 30 histogram bins) are computed and included on the figures. The LSE was computed as; $LSE = \sum (p - data)^2$ where p is the computed PDF fit for the data histogram bin centers. Also, the scintillation index, σ_I^2 given as σ_B^2 in equation (10), and distance are included with each figure. The C_n^2 values were estimated from a near inline scintillometer positioned on the beach between the tower and the research vessel, Chessie.

Low Turbulence Propagation - ($C_n^2 \sim 1.5 \cdot 10^{-14} \text{ m}^{-2/3}$)

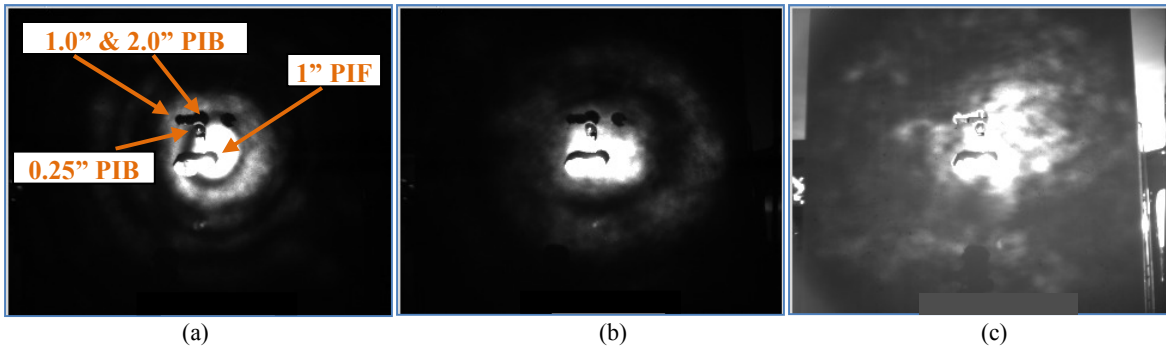
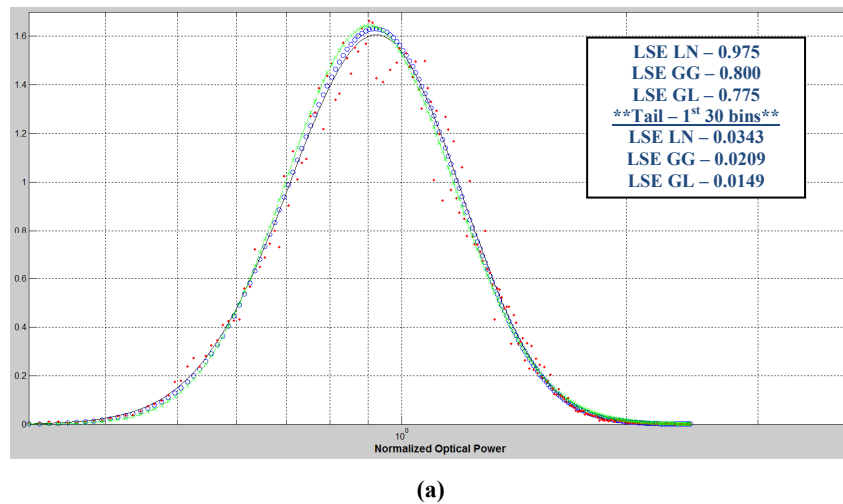
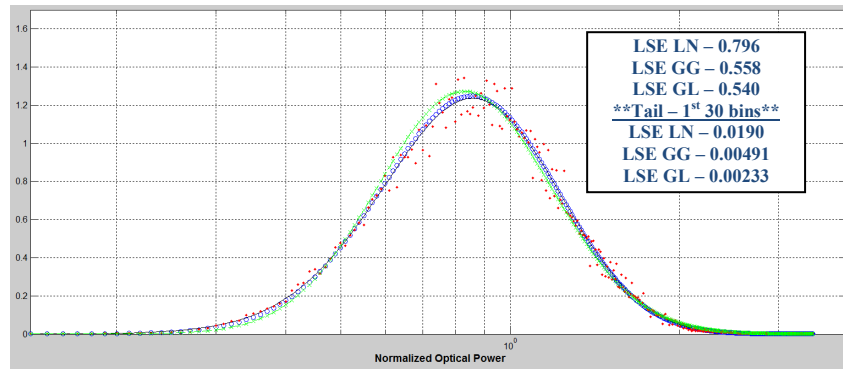
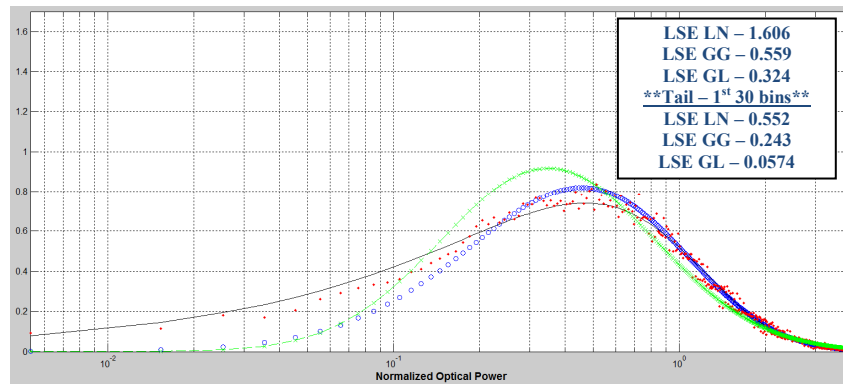


Figure 3 – IR spatial profiles of the beam at distances a) ~5.1 km, b) ~10.7 km, c) ~17.8 km





(b)

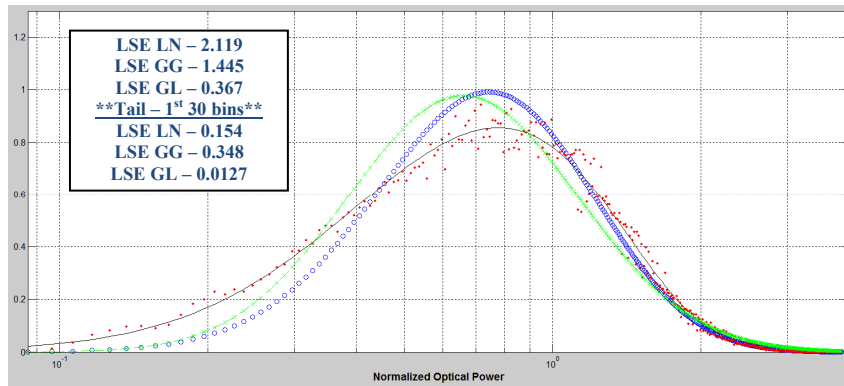


(c)

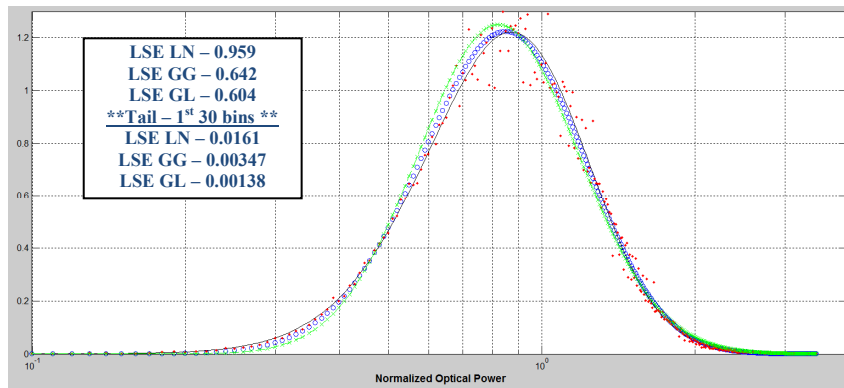
Figure 4 – PDF/Histogram for Low Turbulence Propagation using a 1.0” Power-in-Fiber (PIF) AO detector at 1550 nm. Data Histogram (Red Dots ●), Lognormal (Green --- x), Gamma-Laguerre (Black Solid –), Gamma-Gamma (Blue ○).

- (a) Distance ~5.1 km, $\sigma_I^2 = 0.066174$ **data notes: SixthRun, data block 23**
- (b) Distance ~10.7 km, $\sigma_I^2 = 0.12344$ **data notes: SixthRun2, data block 29**
- (c) Distance ~17.8 km, $\sigma_I^2 = 0.63497$ **data notes: SixthRun4, data block 4**

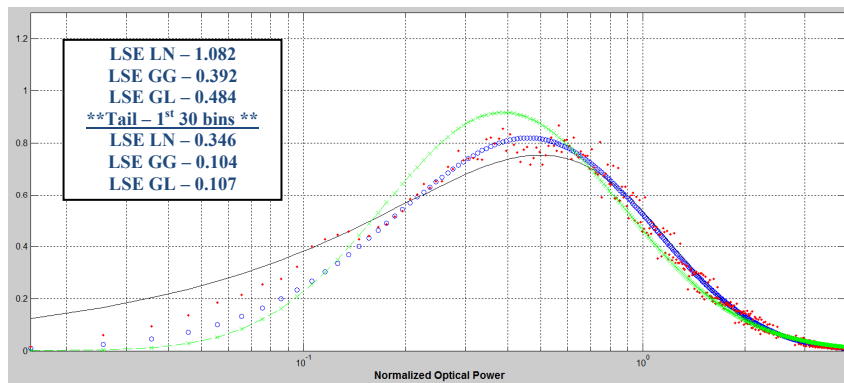
Notes on the data in figure 4. Excellent overlap of all three modeled PDFs with histogram is demonstrated out to 10.7 km. As σ_I^2 rises from 0.066 to 0.63 the histogram and PDF models spreads out. The GL PDF model had the overall best LSE fit across the data set with excellent agreement in the tails – especially, and notably so at 17.8 km.



(a)



(b)

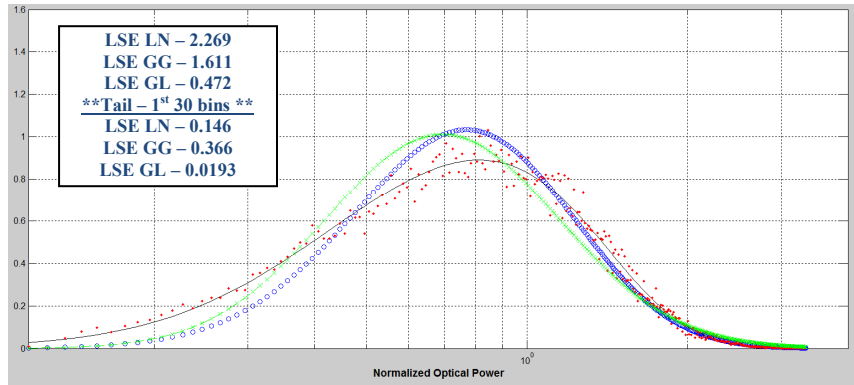


(c)

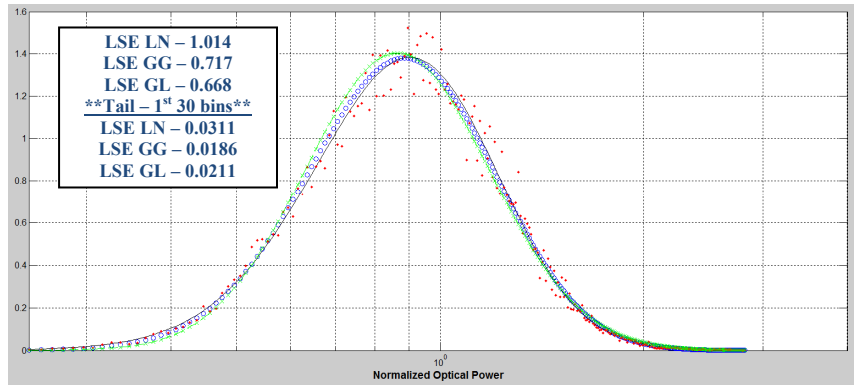
Figure 5 – PDF/Histogram for Low Turbulence Propagation using a 0.25” Power-in-Bucket (PIB) detector at 1550 nm.
 Data Histogram (Red Dots •), Lognormal (Green --- x), Gamma-Laguerre (Black Solid –), Gamma-Gamma (Blue o).

- (a) Distance ~5.1 km, $\sigma_I^2 = 0.23775$ ***data notes: SixthRun, data block 23***
- (b) Distance ~10.7 km, $\sigma_I^2 = 0.12948$ ***data notes: SixthRun2, data block 29***
- (c) Distance ~17.8 km, $\sigma_I^2 = 0.63193$ ***data notes: SixthRun4, data block 4***

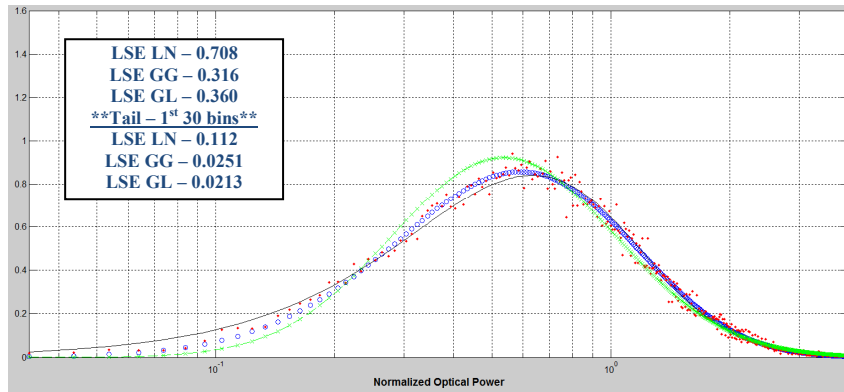
Notes on the data in figure 5. The noticeable spread of distributions and data at short distance (5.1 km) in this case is believed to be due to the PIB detector capturing only the fringes of the beam as can be seen in figure 3a. This can also be seen in the reduction in scintillation index, $\sigma_I^2 - 0.24$ at 5.1 km to 0.13 at 10.7 km. As in figure 4, excellent overlap of all three modeled PDFs with data is observed at the 10.7 km distance with the GL model having the best LSE fit. At the 17.8 km distance, the GG PDF model has the best, but nearly identical LSE tail fit as the GL model - 0.104 tail LSE for the GG compared with 0.107 tail LSE for the GL. Additionally, the GL has an excellent overall fit for the 5.1 km distance where the data captured was in the fringes of the beam. This demonstrates a potential high level of robustness by the GL model to data collected off of beam center.



(a)



(b)



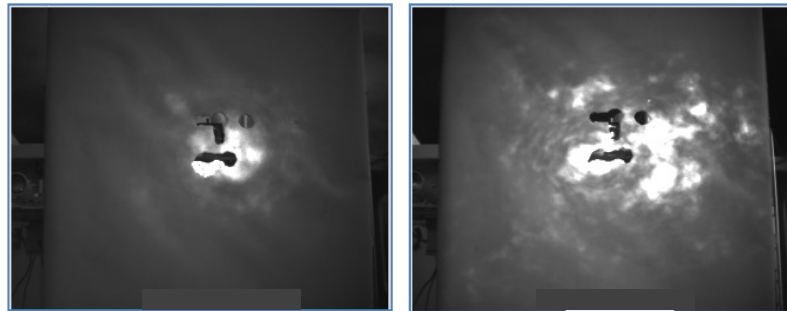
(c)

Figure 6 – PDF/Histogram for Low Turbulence Propagation using a 1.0'' Power-in-Bucket (PIB) detector at 1550 nm. Data Histogram (Red Dots •), Lognormal (Green --- x), Gamma-Laguerre (Black Solid –), Gamma-Gamma (Blue o).

- (a) Distance ~5.1 km, $\sigma_I^2 = 0.20886$ ***data notes: SixthRun, data block 23***
- (b) Distance ~10.7 km, $\sigma_I^2 = 0.096706$ ***data notes: SixthRun2, data block 29***
- (c) Distance ~17.8 km, $\sigma_I^2 = 0.41698$ ***data notes: SixthRun4, data block 4***

Notes on the data in figure 6. A near identical analysis to that given for figure 5 also applies for the 1.0'' PIB detector where we see the same off beam center trending at 5.1 km with an excellent LSE fit by the GL model. The differences seen in this case are that we see a better overall LSE fit by the GL model at 10.7 km, with the GG model just passing the GL model in the tail LSE. For the 17.8 km case we see just the opposite, the GG model has the better overall LSE fit but is just passed by the GL model in the tail LSE fit. Ignoring off beam center challenges with the 5.1 km data set, all three models deliver decent overall fits for the 10.7 km and 17.8 km distance cases.

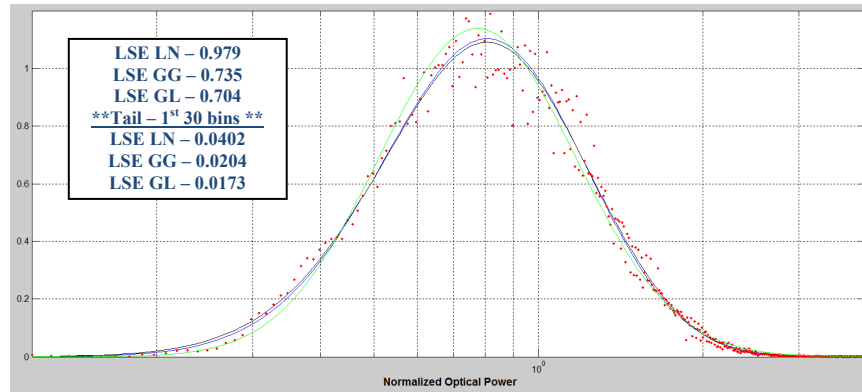
Low-Moderate Turbulence Propagation – ($C_n^2 \sim$ fluctuations between $2 \cdot 10^{-14}$, $8 \cdot 10^{-15}$, and $4 \cdot 10^{-14} \text{ m}^{-2/3}$)



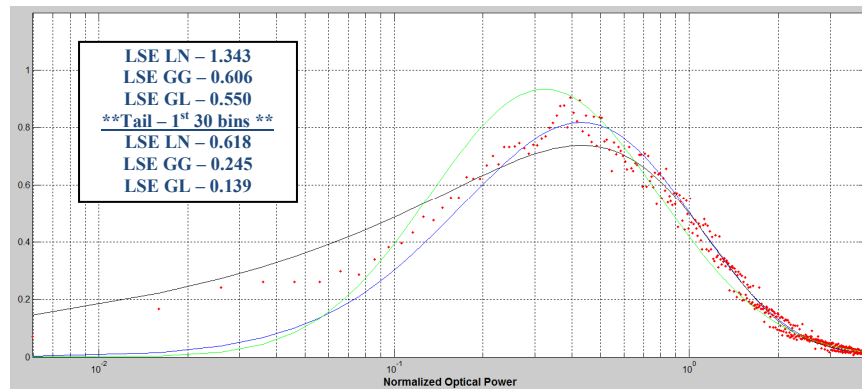
(a)

(b)

Figure 7 – IR spatial profiles of the beam at the distances a) ~6.9 km, b) ~10.5 km



(a)



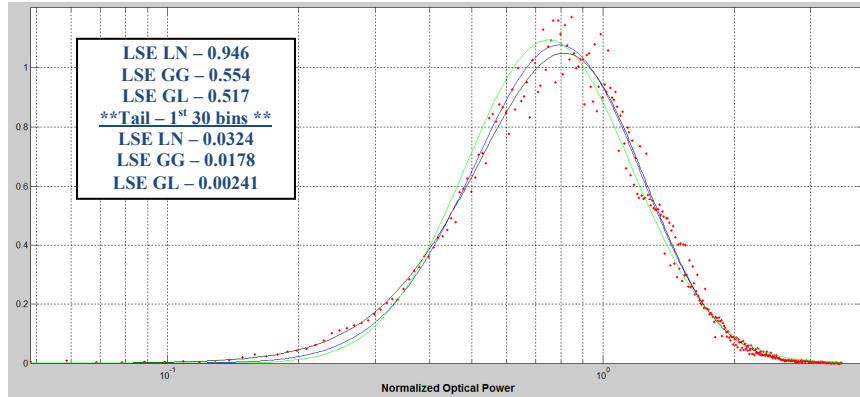
(b)

Figure 8 – PDF/Histogram for Low-Moderate Turbulence Propagation, 1.0” Power-in-Fiber (PIF) AO detector at 1550 nm. Data Histogram (Red Dots ●), Lognormal (Green --- x), Gamma-Laguerre (Black Solid –), Gamma-Gamma (Blue ○).

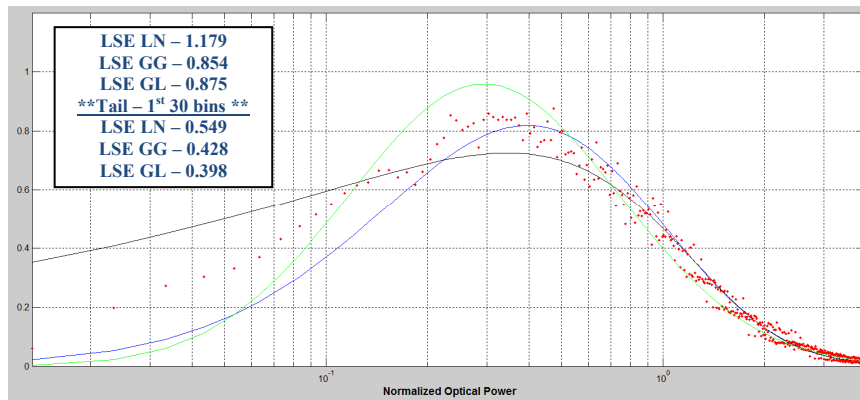
(a) Distance ~6.9 km, $\sigma_I^2 = 0.1715$ **data notes: run12, data block 30**

(b) Distance ~10.5 km, $\sigma_I^2 = 0.70611$ **data notes: run14, data block 7**

Notes on the data in figure 8. Nice overall fit between the distributions at 6.9 km with the GL PDF model having the best overall LSE data fit. Noticeably the GL model appears to underestimate the peak of the data, especially at 10.5 km. This point of underestimating the peak of the data is made by Barakat in his paper on the GL model [6], and we can see it in the fit to the data. That being said, the GL model appears to still have the best overall LSE fit as well as tail LSE fit to the data. These comments also apply to figure 9 on the next page with the exception that the GG model has the best overall LSE fit for the 10.5 km case.



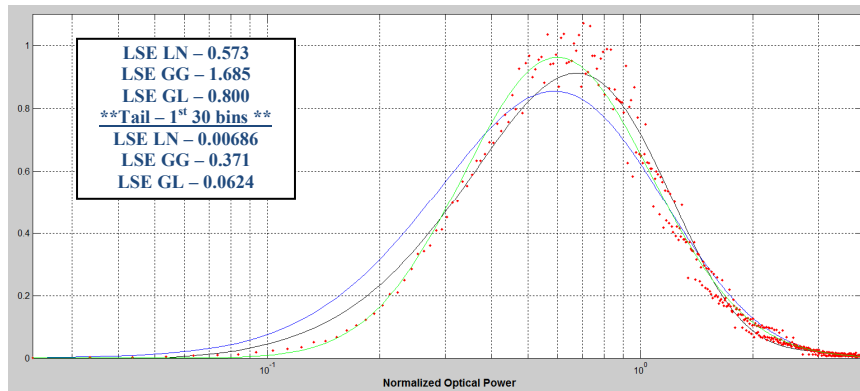
(a)



(b)

Figure 9 - PDF/Histogram for Low-Moderate Turbulence Propagation, 0.25" Power-in-Bucket (PIB) detector at 1550 nm.
Data Histogram (Red Dots •), Lognormal (Green --- x), Gamma-Laguerre (Black Solid -), Gamma-Gamma (Blue o).

- (a) Distance ~6.9 km, $\sigma_I^2 = 0.18443$ ***data notes: run12, data block 30***
- (b) Distance ~10.5 km, $\sigma_I^2 = 0.7895$ ***data notes: run14, data block 7***



(a)

Figure 10 - PDF/Histogram for Low-Moderate Turbulence Propagation, 1.0" Power-in-Bucket (PIB) detector at 1550 nm.
Data Histogram (Red Dots •), Lognormal (Green --- x), Gamma-Laguerre (Black Solid -), Gamma-Gamma (Blue o).

- (a) Distance ~6.9 km, $\sigma_I^2 = 0.43552$ ***data notes: run12, data block 30***

Notes on the data in figure 10. The distinguishing characteristic of this case is that the Lognormal model has a significantly closer fit to the data than the other models. This makes sense as discussed in [11] in that the 1.0" PIB detector experiences more aperture averaging than the other detectors discussed so far.

5. DISCUSSION

Low turbulence data set (figures 4 - 6). At first glance one is immediately drawn to the near overlap of all three models (LN, GL, GG) for the 1.0" PIF AO at 5.1 km and 10.7 km. This is also seen for the 0.25" and 1.0" PIB detectors at 10.7 km. As discussed previously, the fact that the models do not show significant overlap with the data at 5.1 km is potentially due to the PIB detectors capturing just the fringes of the beam (see fig. 3) at this range. Also, as mentioned, the GL model shows an impressive fit to the data in this off beam center situation, and especially in the tail.

The good LN fit to the data at low turbulence supports the historical use of the LN for areas of weak irradiance fluctuations as discussed in [11]. Additionally, while the LN provides a good fit, the GG and GL still fit the data better overall in this turbulence regime and this is supported theoretically in that the PDF cannot truly be LN through retaining perturbation terms up to second order in the Rytov approximation [11].

Low-Moderate turbulence data set (figures 7 – 10). Of immediate note in this turbulence regime is that the 1.0" PIF Adaptive Optics and 0.25" PIB detector distributions are nearly identical across the spectrum. This is curious as one might reasonably expect additional aperture averaging to occur across the 1.0" PIF AO detector vs. the 0.25" PIB detector, and thus have a different distribution of data. More study needs to be done in this area, but one possibility is the effect of the single-mode fiber serving as a spatial frequency filter for the focused light collected in the 1.0" PIF AO detector. This spatial filtering effect is discussed in a number of papers on stellar interferometry, reference [12] as one example. Additionally, Dikmelik and Davidson [13] discuss the effect of increasing turbulence levels and distance on fiber-coupling efficiency to a single-mode fiber in the context of a reduced spatial coherence radius. That being said, an excellent Lognormal fit is seen with the 1.0" PIB detector (figure 10) case as is expected and discussed in [11].

Detector size. For the data collected, the approximate spatial coherence radius as computed from [10] reduces to ~0.5 cm after a few kilometers. This value is significantly less than the apertures used in this experiment with the possible exception of the 0.25" PIB (radius of ~0.3 cm). From the theory on aperture averaging as discussed in [11], the fastest fluctuations caused by small scale sizes average out, this leads to the measured scintillation being produced by scale sizes larger than the aperture. Additionally, a sharp decrease in scintillation occurs as the aperture size reaches the size of the spatial coherence radius. Therefore, in stronger turbulence, if the small-scale scintillation is mostly averaged out, this should shift the PDF toward the distribution of the large-scale fluctuations which would be more LN. This is born out in our data for the low-moderate case where we see that the LN has a better fit for the 1.0" PIB detector case (see figure 10).

6. CONCLUSIONS

In summary, the data collected for an IR beam at 1550 nm using a commercially available adaptive optics terminal, and multiple PIB sensors was compared to three PDF models, the Lognormal (LN), Gamma-Gamma (GG), and the Gamma-Laguerre (GL) for a maritime free space optical channel under varying degrees of optical turbulence and at varying distances of optical propagation. In most cases for this experimental data set and analysis, the GL PDF model provided best or near best LSE fit to the data histogram. This was especially the case in the tails of the distributions at low and low-moderate turbulence. Additionally, the GL PDF model showed robustness to data collected off of beam center. These results are in alignment with experimental studies performed at the United States Naval Academy where data was collected over land and over water at short distance (~400 m) and as highlighted in conference papers [8,9].

7. REFERENCES

- [1] J.C. Juarez, J. E. Sluz, C. Nelson, M. B. Airola, M. J. Fitch, D. W. Young, D. Terry, F. M. Davidson, J. R. Rottier, and R. M. Sova, "Free-space optical channel characterization in the maritime environment," Proc. SPIE 7685, (2010)
- [2] S. Das, H. Henniger, B. Epple, C. I. Moore, W. Rabinovich, R. Sova, and D. Young, "Requirements and Challenges for Tactical Free-Space Lasercomm," Milcom, (2008).
- [3] K.J. Mayer, C.Y. Young, "Effect of atmospheric spectrum models on scintillation in moderate turbulence", *J.Mod. Opt.* **55**, 1362-3044 (2008)
- [4] J.C. Juarez, J. E. Sluz, C. Nelson, M. B. Airola, M. J. Fitch, D. W. Young, D. Terry, F. M. Davidson, J. R. Rottier, and R. M. Sova, "Free-space optical channel characterization in the maritime environment," SPIE Conference presentation, (2010)
- [5] Aitchison, J. and Brown, J. A. C., "The Lognormal Distribution," Cambridge University Press, (1957)
- [6] R. Barakat, "First-order intensity and log-intensity probability density functions of light scattered by the turbulent atmosphere in terms of lower-order moments," *J. Opt. Soc. Am.* **16**, 2269 (1999)
- [7] M. A. Al-Habash, L. C. Andrews, and R. L. Phillips, "Mathematical model for the irradiance probability density function of a laser beam propagating through turbulent media," *Opt. Eng.* **40**, 1554-1562 (2001)
- [8] Svetlana Avramov-Zamurovic, Olga Korotkova, and Reza Malek-Madani, "Probability density function of fluctuating intensity of laser beam propagating in marine atmospheric turbulence," Proc. SPIE 7924,(2011).
- [9] Olga Korotkova, Svetlana Avramov-Zamurovic, and Reza Malek-Madani, "Laser beam characterization of propagation through a marine atmospheric channel," 13th Annual Directed Energy Symposium, (2010).
- [10] L. C. Andrews and R. L. Phillips, *Laser Beam Propagation through Random Media*, 2nd edition SPIE Press, Bellingham, WA, (2005).
- [11] F. Stromqvist Vetelino, C. Young, L. Andrews, and J. Reclons, "Aperture averaging effects on the probability density of irradiance fluctuations in moderate-to-strong turbulence," *Applied Optics*. Vol. 46, No. 11, 2099-2108 (2007)
- [12] C. Ruilier, F. Cassaing, "Coupling of large telescopes and single-mode waveguides: application to stellar interferometry," *J. Opt. Soc. Am. A* Vol. **18**, No. 1, (2001)
- [13] Y. Dikmelik, F. M. Davidson, "Fiber-coupling efficiency for free-space optical communication through atmospheric turbulence," *Applied Optics*. Vol. 44, No. 23, 4946-4952, (2005)